JOURNAL OF MATERIALS SCIENCE 16 (1981) 3437–3446

Indentation plasticity and fracture of Si_3N_4 ceramic alloys

M. H. LEWIS
Department of Physics, University of Warwick, Coventry, UK
R. FUNG, D. M. R. TAPLIN
University of Waterloo, Ontario, Canada

The response of a series of one- and two-phase β-Si_3N_4 ceramic alloy surfaces to sharp diamond microindentation has been examined by optical and electron microscopy. The microhardness (H), which obeys the load-independent relation $H = \alpha P/a^2$ (where P and a are load and indent size, respectively) is nearly constant within the alloy series, indicating a retention of high covalency at large (Al and O) substitution levels. Indentation results from severe localized plasticity which is characterized by the operation of the dominant dislocation Burgers vector $a[0\,0\,0\,1]$ in the hexagonal β lattice. The severe anisotropy in plasticity induces grain-boundary microcracking which is believed to nucleate median cracks which propagate away from the plastic zone on symmetry planes beneath the indenter. The relation between load, median crack size (c) and fracture toughness (K_c) is of the form, K_c = constant $(P/c^{3/2})$ predicted theoretically. Values of K_c rank correctly with those from notched-beam measurements, but there is uncertainty about the value of the constant.

1. Introduction

1.1. Ceramic alloys

The use of Al as an "alloying" element which induces a simultaneous solubility for oxygen in the Si_3N_4 structure has now been convincingly demonstrated as an effective means for improvement of high-temperature mechanical properties of polycrystalline ceramics. Hence, it has been demonstrated [1–4] that by hot-pressing a ceramic of "balanced" composition $Si_{6-x}Al_xO_xN_{8-x}$, with a small addition of MgO to enhance liquid phase sintering kinetics, a single phase product is formed without deleterious grain boundary silicate phase residues. These ceramic alloys undergo a grain-boundary diffusional creep deformation without cavitation and exhibit a remarkable resistance to subcritical crack growth. These related properties are far superior to existing commercial Si_3N_4 ceramics and represent an important step in the evolution of such ceramics which should influence their engineering applications.

The observation of an oxidation induced change in diffusional creep rate for these ceramic alloys has been identified with an increased activation energy for grain-boundary diffusion [2, 3]. This is the result of an outward diffusion of segregated metallic ions which are residual components of the liquid silicate sintering aid. The process is believed to result in an increased primary (covalent) bond density at grain boundaries with consequent reduction in diffusivity for the crystal components.

These high-temperature properties are dominated by intrinsic microstructural variables, e.g. the presence or absence of potential cavity nuclei in the form of silicate residues and the variation in grain boundary cohesion and diffusivity with segregated residual ions. It is unlikely that the fracture stress at low temperatures will be similarly influenced in view of its major dependence on critical flaw size and the mixed inter- and transgranular fracture mode. However, it is of interest to examine the effect of these intrinsic variables on low-temperature plasticity and fracture phenomena such as that under conditions of surface indentation and abrasion. These phenomena

0022–2461/81/123437–10$03.00/0

TABLE I

Specimen number	Approximate value of x in $Si_{6-x}Al_xO_xN_{8-x}$	Treatment	Microstructure
1	1	As hot-pressed	Single phase + grain boundary segregation
2	1	As (1)+ 1000 h at 1400° C	Single phase desegregated
3	1	As (4)+ 1000 h at 1400° C	Single phase desegregated
4	1	As hot-pressed	Single phase + glassy triple-junction residues
5	2	As hot-pressed	Single phase + minor impurity residues at grain boundaries
6	4	As hot-pressed	
7	0.5	Pressureless sintered + 5 h at 1400° C	two-phase β' + YAG

are of importance in relation to engineering applications requiring high hardness and wear resistance such as in bearings, metal cutting, abrasion and rock-drilling.

A new range of two-phase Si–Al–O–N ceramic alloys, which may be fabricated by pressureless sintering, has recently been developed.* Their microstructures consist of β' crystals of low substitution level ($x < 0.5$ in $Si_{6-x}Al_xO_xN_{8-x}$) together with a minor matrix phase which may be either a glassy or crystalline transformation product of the liquid silicate sintering medium [5, 6]. One of these, in which the matrix may be crystallized to silicon substituted yttrium aluminium garnet (YAG) [6], is the basis for a new metal cutting ceramic. It is of particular interest, therefore, to compare the low-temperature hardness, microplasticity and fracture behaviour of this ceramic with the range of single phase Si–Al–O–N ceramics.

1.2. Indentation and abrasion

The deformation and fracture behaviour of a ceramic surface under small-scale contact with a sharp indenter may be related to the macroscopic mechanical properties of the bulk ceramic. The indent size in a crystalline ceramic is related to its plastic flow stress and may be also used in estimating relative ease of dislocation motion on different systems for assymmetric indentations on single crystal surfaces [7, 8]. A more intensive recent activity has been the application of fracture mechanics analyses to relate the elastic–plastic stress field to crack development and hence to such properties as fracture toughness, abrasion and wear resistance [9–14].

Cracks in sharp indentation experiments may be classified either as "median vent" or "lateral vent"; the former nucleate in the deformed volume and propagate on symmetry planes normal to the surface. Lateral vent cracks form during the unloading sequence due to residual stresses between the elastic and plastic zones and propagate nearly parallel to the surface. Lateral vent cracks may emerge at the surface and provide a mechanism for surface removal of material in abrasive contact. However, precise analysis is only available for median cracks, which serves as a simple means for measuring fracture toughness (K_c) from the surface traces of emergent cracks visible at the corners of pyramid indentations [12–14].

The objectives of this paper are:

(a) To determine the validity of the indentation fracture mechanics method for measuring K_c, by comparison with independent measurements from notched beam tests.

(b) To compare the indent size–load relations for the series of ceramics and to estimate the variation in flow stress with ceramic alloy composition.

(c) To determine the geometry of microplasticity in relation to crystal structure and to correlate this with ease of crack nucleation and hence in susceptibility to abrasion.

2. Materials and experimental techniques

2.1. Si_3N_4 alloys

Nominally single-phase β'-Si–Al–O–N ceramic alloys with varying Al and O substitution levels (Table I) have been prepared by hot-pressing using a 1 wt % MgO sintering aid.

Some of the alloys have also been heat treated

*These are known as SYALON ceramics, a trade name of Lucas Industries Ltd.

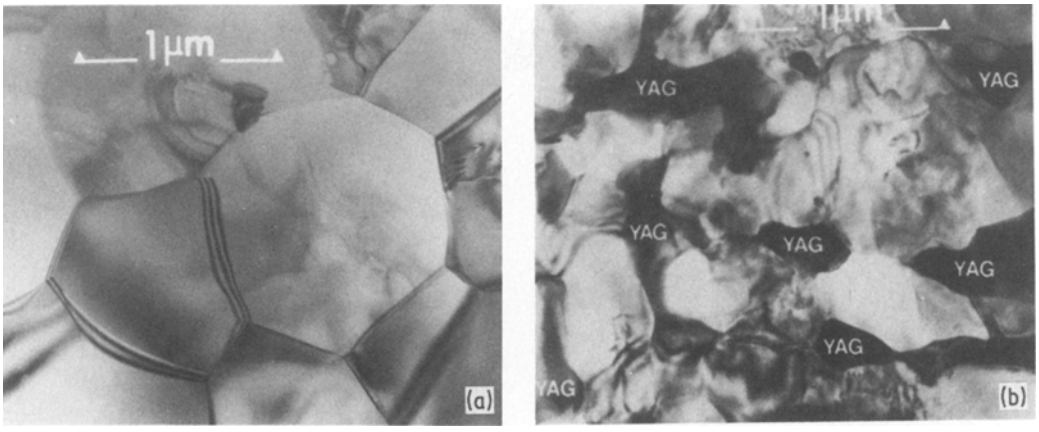

Figure 1 Examples of microstructure in electron transparent sections of (a) single-phase β' and (b) two-phase (β' + YAG) Si–Al–O–N ceramics.

in an oxidizing atmosphere to effect grain-boundary desegregation with a consequent change in high-temperature creep and fracture behaviour described previously [2–4]. An additional alloy, prepared by pressureless sintering, has been studied after a heat treatment which induces crystallization of the matrix from glass to YAG [6]. Examples of the one- and two-phase microstructures are reproduced in Fig. 1.

Specimens for indentation have been diamond cut as 3 mm thick tablets and polished to 1 μm diamond paste.

2.2. Indentation analysis

The polished specimen surfaces were micro-indented with a Vickers pyramid diamond with loads between 50 and 1500 g. A minimum of ten indents were made for each load and the loading cycle was standardized with a period of 10 sec at full load. The size of indent diagonal and median crack surface trace (Fig. 2a and c, respectively) were measured with a micrometer eye-piece on a Zeiss Ultraphot optical microscope. A check on the median crack size was made at higher resolution in a scanning electron microscope. While the fracture mechanics analysis relation for K_c uses the subsurface crack depth, this cannot be measured in opaque ceramics and it has been shown [12, 15] that the latter is nearly equivalent to the surface trace value of c which may be more conveniently measured.

A study of subsurface plasticity and associated crack nucleation was made on multiply-indented polished slices, 0.5 mm in thickness. The slice was subsequently ground to ~ 100 μm when attached to a glass slide by its indented face. A 3 mm brass ring was glued to the specimen with epoxy resin before detachment from the slide. The ring-mounted specimen was thinned by ion-beam erosion until multiple perforation occurred at the indent sites. The erosion rate of the two faces was

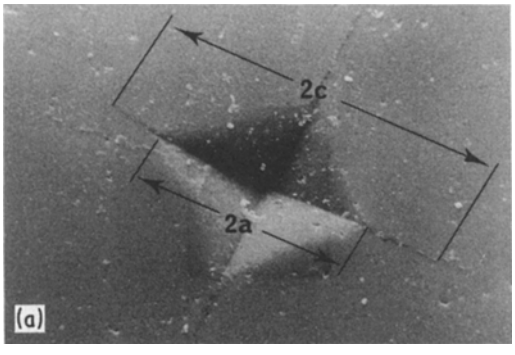

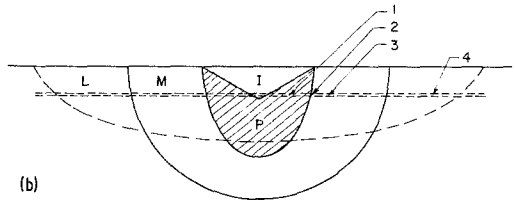

Figure 2 (a) SEM of a Vickers indentation defining indent and median crack parameters "a" and "c", respectively. (b) Cross-sectional diagram of an indent (I) parallel to a median crack plane, illustrating the relation between plastic zone (P), median crack (M), lateral crack (L) and the approximate positions (1, 2, 3) of the electron microscope images (Fig. 4) in the section parallel to the specimen surface (shown as broken parallel lines).

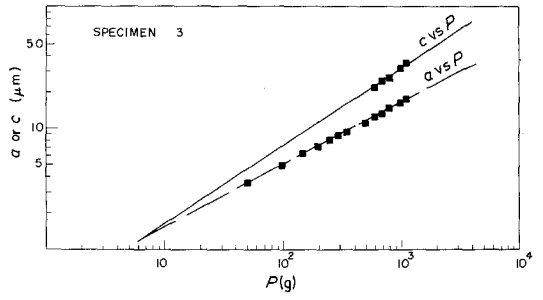

Figure 3 Logarithmic plots of load against indent size (a) or load against median crack size (c) for one of the ceramic alloys.

adjusted such that the electron transparent area (shown schematically by broken parallel lines in Fig. 2b) traversed both the indented volume (I) and the peripheral plastic zone (P) in addition to the median crack (M). Indent loads were selected such that the median crack was just propagated to the surface and was well below the lateral vent (L) threshold. In this way accidental fragmentation of the electron transparent area was minimized. The indented areas were conveniently located using either scanning electron microscopy (SEM) or scanning transmission electron microscopy (STEM) before a detailed study in the same instrument using conventional transmission electron microscopy (CTEM).

3. Indentation mechanisms

3.1. Plasticity and crack nucleation

The anticipated relationship between load (P) and residual indent size (a) is:

$$P/a^2 = \alpha H, \qquad (1)$$

where α is a dimensionless indenter shape factor and H is the contact pressure which is a measure of the material "hardness". The logarithmic a against P plots have a mean gradient of 0.5 ± 0.016, an example of which is reproduced in Fig. 3 and compared with the different c against P relationship discussed later. The variation in hardness H with ceramic alloy substitution level is extremely small; approximately a 5 and 10% reduction in going from $x = 1$ to 2 and 4, respectively. The mechanism for indentation is that of plastic flow via dislocation motion and these observations show that the variation in Peierls stress and hence in degree of bond covalency changes little with Al and O substitution. The two-phase $\beta' + \text{YAG}$ ceramic has, within error limits, a similar hardness indicating that the interconnected β' phase plasticity is again the dominant factor. This is to be expected in a microstructure in which the YAG phase occupies $< 10\%$ by volume and the β' grain size is small in relation to the indentation. This is in contrast with the differences in high-temperature creep deformation between single- and two-phase ceramics where the presence of the YAG phase changes the rate controlling mechanism [16].

A detailed study of the plastic zone beneath the indented surface and the transition in microstructure into the region of median crack propagation has been made by TEM. The labels 1, 2 and 3 in Fig. 4 refer to approximate positions in the thin section shown schematically in Fig. 2b. In Position 1, within the plastic zone, the dislocation density is such that much overlap in their strain fields occurs, inhibiting individual imaging. However there is a clear preference for uniaxial alignment of dislocations in individual β' grains, dependent on their orientation. Grain boundary microcracks occur on most grain facets and are visible either as narrow openings parallel to the electron beam or in the form of "wedge fringe" or Moiré contrast when inclined to the beam direction. In general, microcracks on individual facets are not interlinked, which indicates that they may form in relief of inhomogeneous plastic stresses during indentation and not as a result of propagation during specimen thinning. The plastic zone extends to $\sim 25\%$ of the indent size beyond the indent surface. The reduction in dislocation density near to the plastic–elastic interface (Position 2) facilitates a precise Burgers vector analysis. In Zone 3 median crack propagation occurs, without plasticity, in a mixed inter- and transgranular mode (Fig. 4).

Analysis of Burgers vectors shows that nearly all grains contain only dislocations with **b** parallel to the c-axis in the hexagonal β' structure. Hence dislocations are invisible when using the (easily identifiable $10\bar{1}0$ prism plane reflections. A clear example of this (taken from Position 2), which shows individual dislocation contrast, is illustrated in Fig. 5. In this grain dislocations are visible as expanding loops with a strong preference for exact screw orientation (i.e. parallel to the c-axis) in the highly covalent crystal. The same alignment occurs in all grains and is explicable via the magnitude of **b** (and hence elastic energy) which increases rapidly with deviation from the c-axis in the hexagonal unit cell with small c/a ratio (Fig. 6). A similar influence has been noted

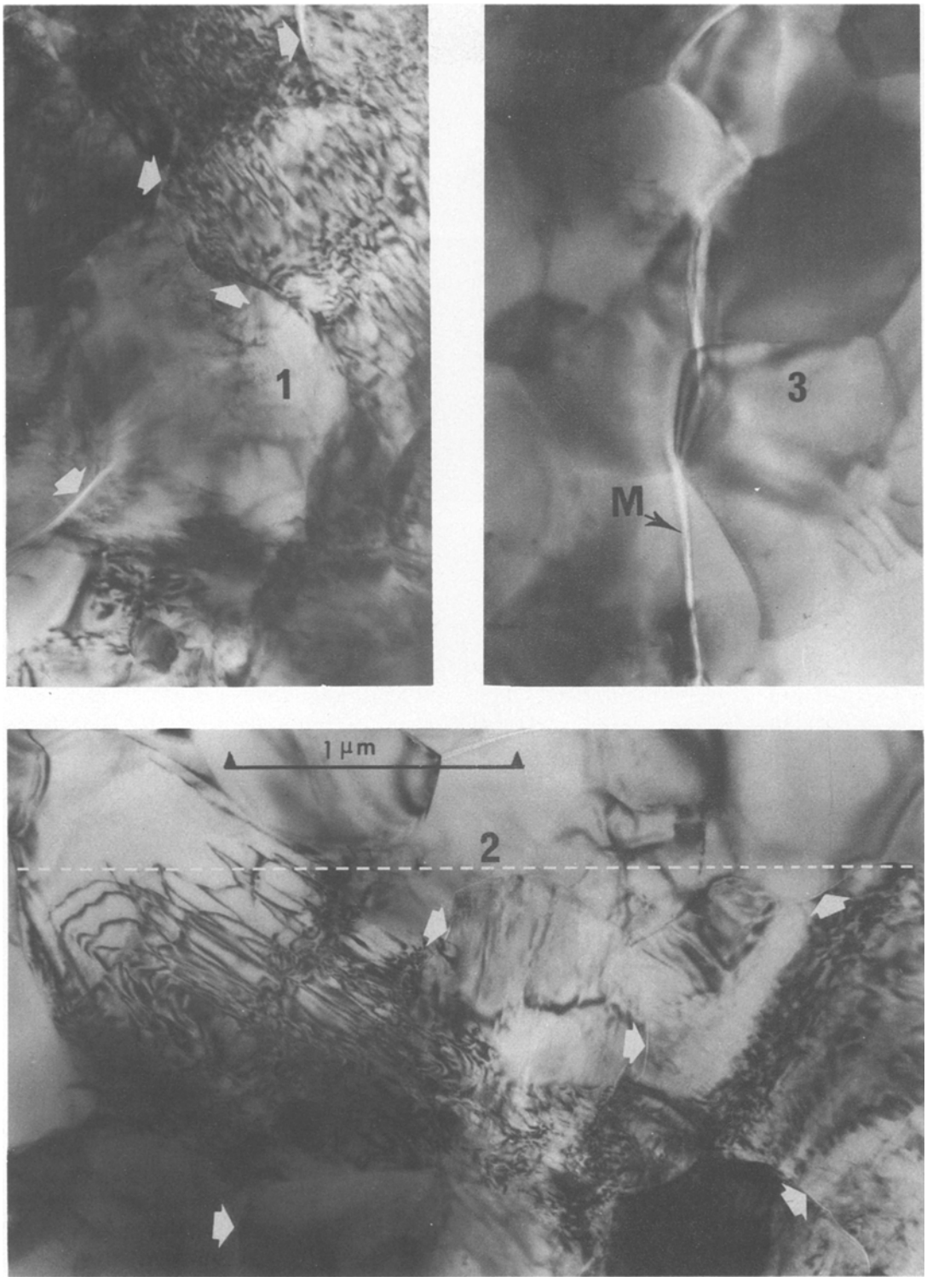

Figure 4 Transmission electron micrographs showing the severely dislocated β' grain structure and grain-boundary microcracking (arrowed) within the plastic indent zone (image 1 and the lower part of image 2). Image 2 shows the plastic–elastic interface (dotted) and image 3 is well removed from the plastic zone and is normal to the plane of the mainly intergranular median crack (M).

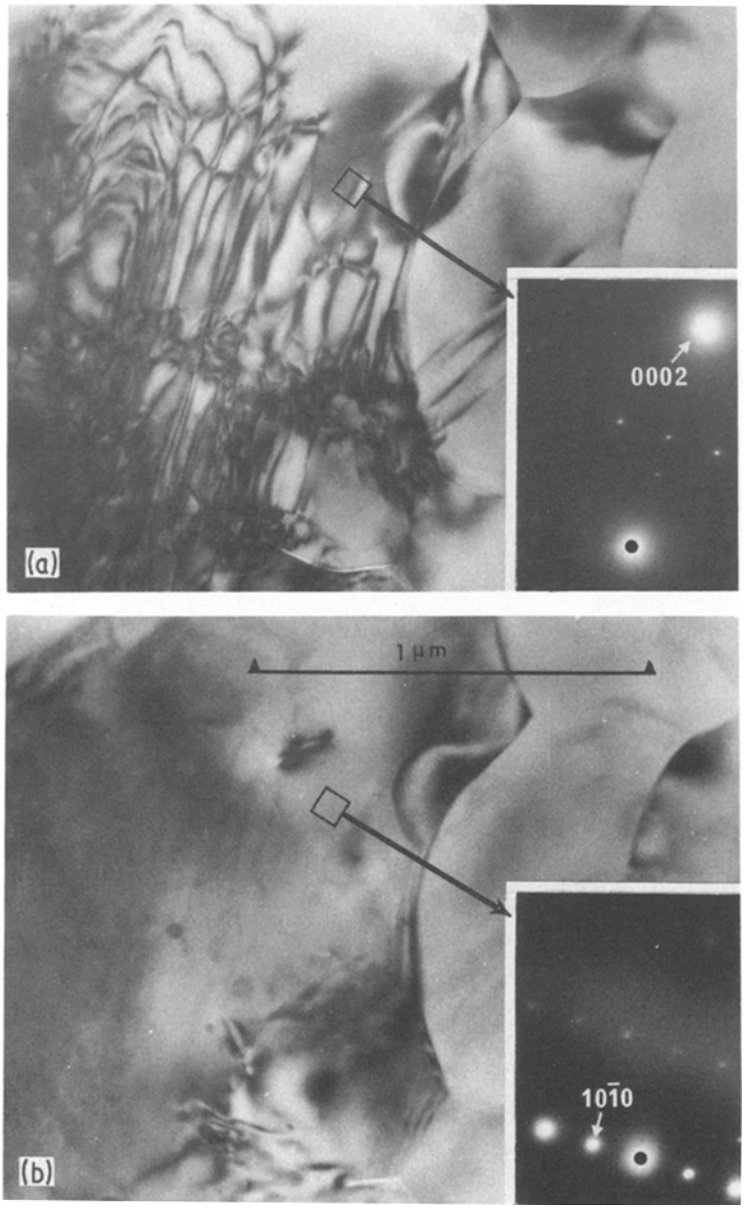

Figure 5 Burgers vector analysis in a β' grain near the periphery of the plastic zone. Dislocations, which are shown to have preferred [0 0 0 1] orientation and a[0 0 0 1] Burgers vector, are (a) imaged with 0 0 0 2 reflections and (b) invisible with prism plane 1 0 $\bar{1}$ 0 reflections. The "stranger" dislocation segments which are imaged in both (a) and (b) must have Burgers vectors inclined to both a- and c-axes (e.g. $\mathbf{b} = a + c$) and are observed in negligible density throughout the plastic zone.

for the occasional dislocations observed in β-Si_3N_4 ceramics compressed at elevated temperatures [17].

The nucleation mechanism for grain-boundary microcracks follows logically from the analysis of unique Burgers vectors in the plastic zone. This is shown schematically in Fig. 6 as the opening of grain boundaries following dislocation pile-up. The absence of five independent slip systems dictates that neighbouring grains cannot undergo the general shape change required to relieve shear stresses in the adjacent crystal. There has been some discussion in the literature on indentation fracture mechanics concerning the origin of median or lateral vent crack nuclei. One possibility is that the increasing elastic stress field "samples" a range of accidental flaw sizes distributed in the material, the largest of which propagates [18]. An alternative is the nucleation of cracks via inhomogeneity in shear stress within the plastic zone [19]. The experimental evidence of extreme plastic anisotropy in the hexagonal crystal indicates that a "nucleation" model is applicable to ceramics of the β-Si_3N_4 type.

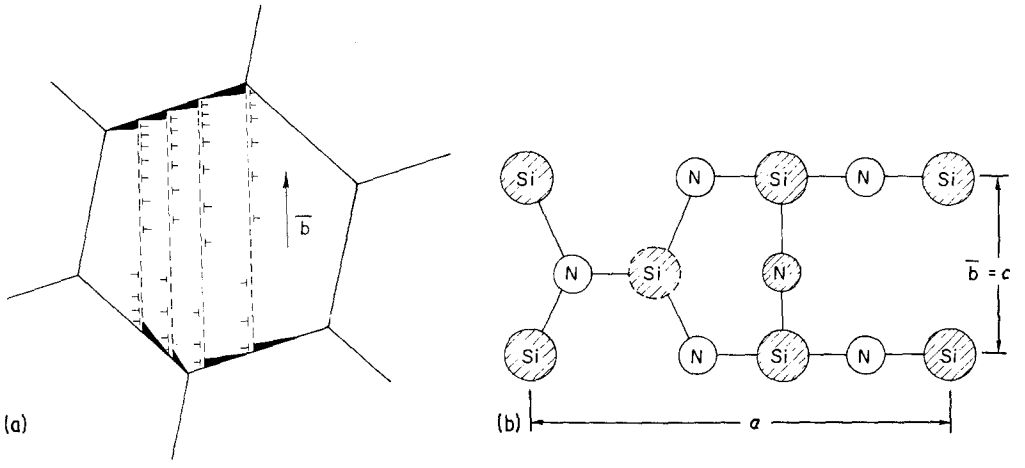

Figure 6 (a) Illustration of the nucleation of grain-boundary microcracks as a result of the operation of a singular dislocation Burgers vector $a[0\,0\,0\,1]$. (b) Projection of a unit cell of the β-Si_3N_4 crystal structure showing the relative sizes of lattice translation vectors in the a and c directions and hence the selection of an $a[0\,0\,0\,1]$ Burgers vector. (Open circles are atoms approximately within the diagram plane, shaded atoms lie above the diagram plane except for that in broken outline.)

3.2. Crack propagation and fracture toughness

Analysis of the propagation of well developed median cracks has been attempted in a number of papers via fracture mechanics. The simplified two-dimensional approach of Lawn and Swain [9] considered the growth of subsurface median cracks in an elastic point-contact stress field and obtained a relation between crack size c and contact load P which contained the fracture toughness parameter, K_c,

$$K_c = \psi_a(P/c)^{\frac{1}{2}}, \tag{2}$$

where ψ_a is a function of various geometrical and material constants (Poissons ratio and hardness). Fig. 3 shows this relationship to be inapplicable to the measurements made here; the logarithmic c–P plots for the whole series of ceramic alloys fit the relationship first derived from dimensional analysis by Lawn and Fuller [12]:

$$K_c = \psi_b(P/c^{\frac{3}{2}}), \tag{3}$$

where $\psi_b = 1/\pi^{3/2} \tan \psi$, and ψ is the indenter half-angle. Examples for the single-phase and two-phase β' ceramics are reproduced in Fig. 7 and Table II is a least squares analysis of the P–c index. There is a satisfactory agreement with the Lawn–Fuller index and this relationship has been used in calculating K_c.

The calculated fracture toughness shows a moderate agreement with the gradation in K_{1c} determined independently from notched beam tests for the three ceramics listed in Table III.

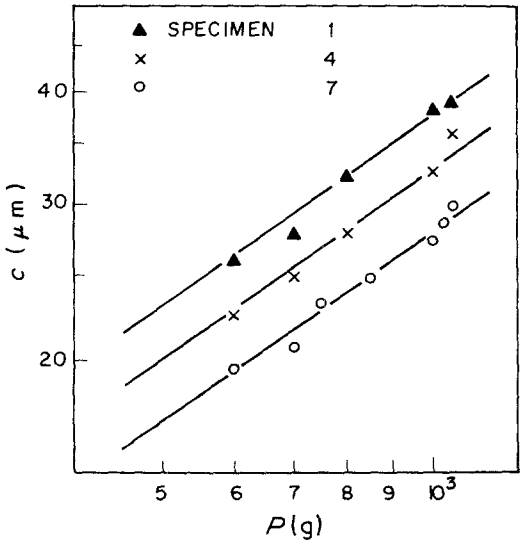

Figure 7 Logarithmic plot of median crack size (c) against load (P) for 3 of the ceramic alloys with lines drawn according to the relation K_c = constant $P/c^{3/2}$.

TABLE II

Specimen	Value of $1/n$ in K_c = const. P/c^n
1	0.727 ± 0.066
2	0.881 ± 0.038
3	0.734 ± 0.016
4	0.764 ± 0.018
5	0.727 ± 0.020
6	0.564 ± 0.014
7	0.700 ± 0.044

TABLE III

Specimen	K_c (indentation) (MPa $m^{\frac{1}{2}}$)	K_c (× 1.4 MPa $m^{\frac{1}{2}}$)	K_{1c} (notched beam or double torsion) (MPa $m^{\frac{1}{2}}$)
1	2.29 ± 0.11	3.21	3.1
2	2.52 ± 0.25	3.53	–
3	2.97 ± 0.09	4.16	–
4	2.77 ± 0.11	3.88	4.7
7	3.53 ± 0.13	4.94	4.9

However, the absolute magnitudes of K_c are too low, differing on average by a factor of 1.4. Hence a more appropriate constant in this relationship would be 0.073 in place of 0.052 ($= 1/\pi^{3/2} \tan \psi$).

The origin of the variation in K_c is believed to be the morphological aspect ratio for the β' crystals which have grown, during hot-pressing or sintering, in different environments. That with the greatest shape elongation in the hexagonal c-axis is the two-phase alloy in which the liquid silicate sintering medium has a comparatively large volume fraction. Hence, β' crystals may grow with greater freedom to demonstrate their marked anisotropy in growth kinetics before impingement. K_c is enhanced because the partially intergranular fracture involves a more tortuous path and resultant "pull-out" of the elongated crystals. There is no evidence for enhancement of K_c due to plasticity of single-phase ceramics, Fig. 4(3), but plasticity in the YAG phase may provide a small additional contribution in two-phase ceramics. The remaining hot-pressed ceramics (Specimens 1 and 4) have previously been shown to contain different residual phase contents which must reflect differences in liquid content during the final stages of sintering and hence small differences in c/a shape ratio. The approach to zero residual phase content for Specimen 1 is the origin of its superior high-temperature properties in comparison with Specimen 4 [2]. It is significant that a small change in K_c occurs on heat treatment of the single-phase ceramics. This must originate from the influence of grain-boundary desegregation on fracture surface energy.

The relationship K_c = constant $P/c^{3/2}$ is well established both for crystalline and non-crystalline ceramics. However, as shown in Table III, absolute levels of K_c suffer from uncertainties in the constant, due to lack of theoretical precision in describing the elastic–plastic stress field. Lawn *et al.* [20] have recently modelled this field as a reversible (elastic) component, which enhances median crack growth during loading, and an irreversible (plastic) component which is important in the final stages of crack growth. The latter is clearly related to material hardness (H) and modulus (E) which are then contained in the revised relationship for K_c:

$$K_c = 0.026(\text{Cot } \psi)^{\frac{1}{2}}(E/H)^{\frac{1}{2}} \cdot P/c^{\frac{3}{2}}, \quad (4)$$

where the constant is appropriate for Vickers indentation geometry, part of which has been empirically determined [20]. Application of this model results in K_c values which are only 4% higher than calculated above, variations in $(E/H)^{1/2}$ within the ceramic alloy series being negligible. Thus it appears that it is necessary to calibrate the geometrical constant for a particular type of material (having a specific surface friction) and indenter. It is inappropriate that Vickers indenters have such large angles ($\psi = 74°$) because of the sensitivity of $\tan \psi$ in this range. For example, a reduction in ψ of only 6° is needed to modify K_c by a factor of 1.4 as previously suggested. Indenters specifically designed for K_c determination with smaller angles between faces, should be considered.

3.3. Abrasive wear

The surface removal of material with multiple point contact (abrasive wear) has been described via a model in which the irreversible or residual stresses due to the plastic zone result in a propagation of cracks parallel to the surface i.e. the lateral vent cracks [11]. This mechanism for surface "chip" formation has been experimentally observed in glasses under conditions of single indentation during the unloading cycle. Lateral cracking was not observed for the series of Si–Al–O–N ceramics under the relatively low indenter loads used to study median cracking. However, a controlled diamond cutting test was conducted to assess their relative susceptibility to abrasive wear. For the same diamond saw condition and pressure the times taken to cut unit cross-sectional areas for the single-phase ceramics varied between 34 and 44 sec; that for the two-

phase ceramic was 80 sec. This marked increase in abrasive cutting resistance may be due to the increased fracture toughness, with contributions from the elongated β' crystal morphology and microplasticity within the matrix phase. An additional factor may be the reduction in density of critical flaws due to the ability to relax interfacial stresses, resulting from β' dislocation pile-up, by matrix microplasticity. It is significant that the YAG matrix crystal structure has cubic symmetry and hence the potential for five independent slip systems. This proposed mechanism for accommodating anisotropy in β' crystal plasticity and suppression of interfacial crack nucleation may be especially effective under low stress abrasion when the indentation misfit stress is below threshold for lateral crack propagation. Under these conditions abrasion occurs via frictional detachment of individual surface grains which have lost cohesion via multiple facet crack nucleation of the type depicted in Fig. 6.

4. Conclusions

(1) The low load Vickers indentation hardness for a range of β' Si–Al–O–N ceramics conforms to the load independent relation, $H = \alpha P/a^2$ and exhibits a negligible variation with substitution level for Al and O in Si_3N_4. This may be interpreted as a retention of high average bond covalency which should not discourage the development of highly substituted alloys such as $SiAl_2O_2N_2$.

(2) A study of the plastic indentation zone has determined that β' crystals exhibit gross plastic shear anisotropy with a singular Burgers vector $a[0001]$ in the hexagonal lattice. This lack of multiplicity in slip systems infers the loss of cohesion at grain boundaries in the highly deformed zone. Such microcracks have been directly observed in single-phase β' ceramics and form nuclei for median crack propagation away from the plastic zone.

(3) Median cracking at indenter loads between 500 and 1500 g follows a relation of the type, K_c = constant $(P/c^{3/2})$. The calculated values of fracture toughness, K_c, for the range of alloys are similarly ranked to those determined from notched beam tests. The absolute values are systematically lower by a factor of ~ 1.4 due to uncertainties in the value of the constant which is extremely sensitive to pyramid angle for Vickers indenters. One of the origins for the variation in K_c is believed to be the β' morphological anisotropy which is influenced by the volume of liquid sintering aid.

(4) A simple cutting test shows the two-phase ceramic alloy to be most resistant to diamond abrasion. This may be an influence of the increased K_c on lateral vent crack propagation or on the flaw population induced by β' plastic anisotropy. Hence the probable matrix plastic isotropy may suppress interfacial microcracking.

(5) The subtle differences in grain boundary structure which induce gross variations in high-temperature creep and slow crack growth within the ceramic alloy series are not reflected in their low-temperature indentation plasticity and fracture. This, together with important property differences for two-phase materials emphasizes the need to develop a range of Si–Al–O–N ceramic alloys dependent on their engineering application.

Acknowledgements

The collaboration with the Lucas Group Laboratories, especially Dr R. J. Lumby, in a continuing research programme on Si–Al–O–N ceramics is gratefully acknowledged. Part of this research was carried out during a visit to Warwick University by one of the authors (RF) who wishes to thank Mr G. Smith and Mr M. Thornton for experimental assistance.

References

1. M. H. LEWIS, B. D. POWELL, P. DREW, R. J. LUMBY, B. NORTH and A. J. TAYLOR, *J. Mater. Sci.* **12** (1977) 61.
2. B. S. B. KARUNARATNE and M. H. LEWIS, *ibid.* **15** (1980) 449.
3. *Idem, ibid.* **15** (1980) 1781.
4. M. H. LEWIS and B. S. B. KARUNARATNE, Proceedings of the American Society for Testing of Metals Symposium on Fracture Mechanics Techniques in Ceramics, Chicago, 1980 (ASTM special technical publication, Philadelphia, in press).
5. M. H. LEWIS, A. R. BHATTI, R. J. LUMBY and B. NORTH, *J. Mater. Sci.* **15** (1980) 438.
6. *Idem, ibid.* **15** (1980) 103.
7. C. A. BROOKES, J. B. O'NEILL and B. A. W. REDFERN, *Proc. Roy. Soc.* **A322** (1971) 73.
8. G. MORGAN and M. H. LEWIS, *J. Mater. Sci.* 9 (1974) 349.
9. B. R. LAWN and M. V. SWAIN, *ibid.* **10** (1975) 113.
10. B. R. LAWN and D. B. MARSHALL, *J. Amer. Ceram. Soc.* **62** (1979) 347.
11. A. G. EVANS and T. R. WILSHAW, *Acta. Met.* **24** (1976) 939.
12. B. R. LAWN and E. R. FULLER, *J. Mater. Sci.* **10** (1975) 2016.
13. A. G. EVANS and E. A. CHARLES, *J. Amer. Ceram. Soc.* **59** (1976) 371.
14. S. S. SMITH, P. MAGNUSEN and B. J. PLETKA, Proceedings of the American Society for Testing of Metals Symposium on Fracture Mechanics Tech-

niques in Ceramics, Chicago, 1980 (ASTM special technical publication, Philadelphia, in press).
15. R. H. MARION in "Fracture Mechanics Applied to Brittle Materials", ASTM (STP 678) (American Society for Testing Metals, Philadelphia, 1979) p. 103.
16. M. H. LEWIS, B. S. B. KARUNARATNE, J. MEREDITH and C. PICKERING, in "Creep and Fracture of Engineering Materials", edited by B. Wilshire and D. R. J. Owen (Pineridge Press, Swansea, 1981) p. 365.
17. A. G. EVANS and J. V. SHARP, in "Electron Microscopy and Structure of Materials" edited by G. Thomas, (University of California Press, Berkeley, Calif., 1972) p. 1141.
18. B. R. LAWN and A. G. EVANS, *J. Mater. Sci.* **12** (1977) 2195.
19. J. T. HAGAN, *ibid.* **14** (1979) 2975.
20. B. R. LAWN, A. G. EVANS and D. B. MARSHALL, *J. Amer. Ceram. Soc.*, in press.

Received 6 May and accepted 29 May 1981.